PCCP
Physical Chemistry Chemical Physics

Accepted Manuscript

This article can be cited before page numbers have been issued, to do this please use: I. Bodrenko, M. Ceccarelli and S. Acosta-Gutierrez, *Phys. Chem. Chem. Phys.*, 2023, DOI: 10.1039/D3CP02895J.

ROYAL SOCIETY OF CHEMISTRY

rsc.li/pccp

View Article Online
DOI: 10.1039/D3CP02895J

The mechanism of an electrostatic nanofilter: overcoming entropy with electrostatics

Igor Bodrenko,[1,2] Matteo Ceccarelli,[2,3*] Silvia Acosta Gutierrez[4]

[1]École Normale Supérieure, Département de Chimie – Laboratoire PASTEUR, Paris, France

[2]CNR-IOM, Sezione di Cagliari, Cittadella Universitaria di Monserrato, S.P.8 – km 0.700, 09042 Monserrato (CA), Italy

[3]Department of Physics, University of Cagliari, Cittadella Universitaria di Monserrato, S.P.8 – km 0.700, 09042 Monserrato (CA), Italy

[4]Institute for Bioengineering of Catalonia. Carrer Baldiri Reixac 10-12, 080028 Barcelona, Spain.

corresponding author mail:matteo.ceccarelli@dsf.unica.it; sacosta@ibecbarcelona.eu

Abstract:

General porins are nature's sieving machinery in the outer membrane of Gram-negative bacteria. Their unique hourglass-shaped architecture is highly conserved among different bacterial membrane proteins and other biological channels. These biological nanopores have been designed to protect the interior of the bacterial cell from leakage of toxic compounds while selectively allowing the entry of the molecules needed for cell growth and function. The mechanism of transport through porins is of utmost and direct interest for drug discovery, extending toward nanotechnology applications for blue energy, separations, and sequencing. Here we present a theoretical framework for analysing the filter of general porins in relation to translocating molecules with the aid of enhanced molecular simulations quantitatively. Using different electrostatic probes

in the form of a series of related molecules, we describe the nature of this filter and how to finely tune permeability by exploiting electrostatic interactions between the pore and the translocating molecule. Eventually, we show how enhanced simulations constitute today a valid tool for characterising the mechanism and quantifying energetically the transport of molecules through nanopores.

INTRODUCTION

Transport through biological membranes is a fundamental process for life, permitting the exchange of nutrients/waste products and signalling molecules, or in general transfer of information in and out of cells.[1] While small, hydrophobic or moderately polar molecules are able to diffuse passively and directly across membranes, larger and more polar compounds must use membrane transporters/channels in order to enter the cell successfully. A relevant class of channels is constituted by beta-barrel proteins: the active transporters, known as Ton-B dependent transporters,[2] and the passive channels.[3] These biological nanopores have a key role in many living processes and have been a source of inspiration for recent technological applications,[4,5] in particular DNA sequencing,[6] water treatments,[7] and blue energy.[8]

In the outer membrane (OM) of Gram-negative bacteria, a plethora of different proteins are expressed for the uptake of polar molecules required for bacterial cell growth and function.[9] Many of these systems function upon passive gradient diffusion, but in order to avoid unrestricted and fast access to toxic compounds, they have evolved to develop specificity or sieving mechanisms.[10] Specific channels are an example of this evolution in which the recognition of particular interactions is a key step in molecular permeability, as is the case of aquaporins,[11] sugar-specific channels,[12,13] or other substrate-specific channels like the Occ family from *Pseudomonas aeruginosa)*[14,15] and

View Article Online
DOI: 10.1039/D3CP02895J

Acinetobacter baumannii.[16,17] Conversely, in the case of general porins, such as the Enterobacteriaceae OmpF/OmpC orthologs,[18] the OmpT/U porins from *Vibrio cholera*,[19] and MOMP from *Campylobacter jejeuni*,[20] the role and relevance of specific interactions, binding sites or affinity sites in molecular permeability has been widely debated.[21,22]

Bacterial porins exhibit a very particular architecture, Fig. 1a, highly conserved along the respective bacterial orders (Enterobacteriaceae, Pseudomonadaceae, Vibrionaceae, Campylobacteraceae). These beta-barrel proteins are constricted halfway down the axis of diffusion by one or more internal loops that create the so-called constriction region (CR) (**Fig. 1a**). In addition, this narrow region exhibits a striking charge segregation on opposite sides of the wall (**Fig. 1a**), creating a strong transversal electric field.[23] The CR defines the size exclusion limit for translocation through these channels [24], and it has been finely tuned in order to modulate the permeability of the outer membrane.[25] This constriction is also present in other biological channels like the mitochondrial VDAC[26,27] or the CymA,[28] where the mobile N-terminus element can constrict the lumen when it folds inside.

The fluctuations of the internal loop constricting the lumen of general pores can gate the channel, either spontaneously[29] or upon external stimuli like temperature.[30] However, the size of the channel is not the only parameter controlling molecular permeability: its electrostatic fingerprint plays a key role in stabilising the desolvated form of polar molecules, thereby aiding their translocation.[31,32] Also the ionic species in solution, like the presence of di-cations, can modify the internal affinity site.[33,34] Both the channel fingerprint and the charge distribution of the translocating molecule can be modified to tune molecular permeability, in the former case with applications in nanotechnology,[35] in the latter for microbiology.[36]

Porins like OmpF/OmpC are considered non-specific channels, meaning molecules can permeate by passive diffusion.[21] Notwithstanding, the outer membrane is a system in which permeation is controlled by a combination of influx (porin-mediated) and efflux processes, and it cannot be explained using Fick's law for passive diffusion.[37] Experimentally, single-molecule single-channel electrophysiology experiments can sense the pore-molecule interactions, providing association and dissociation rates for influx.[38] Accumulation assays, can also asses influx when efflux systems are not expressed.[39] Recently, we presented a scoring function[40,41] able to rank compounds according to their ability to permeate through general porins. Our results showed an excellent agreement with accumulation assays and other biophysical and microbiological assays. The scoring function is based on a statistical model for describing the general steric filter of these porins, revealing that its entropic nature is translated in an enthalpic diffusive transport, [42] as well as electrostatic interaction terms (charge and dipole).[39] Here, in order to fully depict the energetic landscape behind the permeability process through bacterial general porins, we have selected a set of related penicillin molecules (**Fig. 1**), with incremental change in charge and electric dipole moment, to study their permeation through the OmpF porin from *Escherichia coli*, a well-characterized biological nanopore, by means of enhanced sampling molecular dynamics. With respect to other groups,[43,44] we explicitly considered two collective variables, namely the position of the diffusing molecule along the axis of diffusion and its orientation. Eventually, we revealed the influence of the electrostatic pore-molecule interactions in fine-tuning permeability and, thus, the molecular transport rates Our results provide useful guidelines for antibiotics design but also enable the designing of artificial pores with particular filtering mechanisms that can be exploited for technological applications.

View Article Online
DOI: 10.1039/D3CP02895J

Results

Selection of molecules

We selected molecules from the penicillin's group to have a series with approximately the same size, and thus the same steric barrier, with incremental charge and electric dipole moment states (**Fig. 1**): the dianionic carbenicillin (electric dipole moment of 12.7 Debye), the anionic benzylpenicillin (electric dipole moment of 18.2 Debye), and the zwitterionic ampicillin (electric dipole moment of 34 Debye). These related compounds have the advantage that for two of the them (ampicillin and carbenicillin) an X-ray co-complex with OmpF is available and will be used to validate our free energy calculations and to discuss the role of high-affinity sites on molecular transport.[22] To note that an OmpF co-complex is also available for a negatively charged molecule fragment, ertapenem.[22] Further, in order to extend the electrostatic properties of our set with a positive molecule, we designed a variant penicillin to obtain a molecule positively charged with the same size as the others. Starting from ampicillin, we substituted a carbon atom of the phenyl ring with a nitrogen, obtaining a cationic molecule, the cationic compound-1, with two positive groups and one negative group. This molecule would be positively charged at low pH. Though, we decided to simulate this low pH form without altering the protonation states of OmpF, thus keeping the same environment for all the compounds. This way, we obtained a series of related compounds with incremental charge (from -2e to +1e) but similar size. Adding the second positive group also increases the electric dipole moment (electric dipole moment of 37 Debye) with respect to zwitterionic ampicillin (electric dipole moment of 34 Debye), providing a series with an incremental dipole moment too.

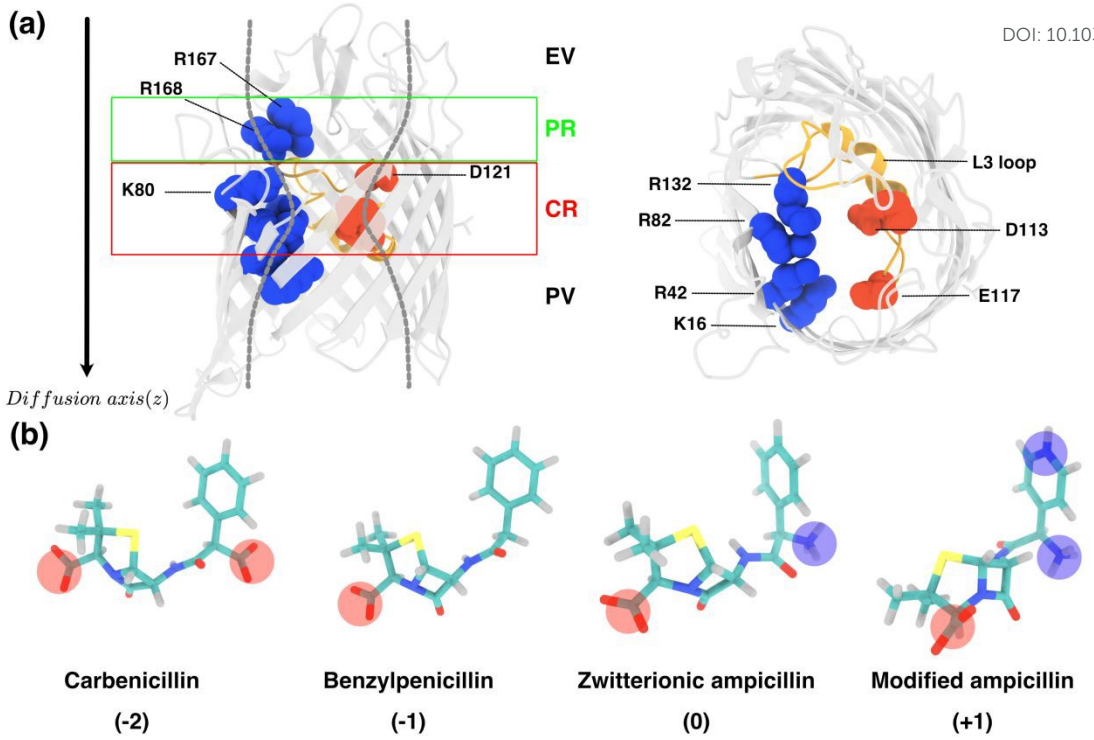

Figure 1. (a): General architecture of Enterobacter porins with highlighted the loop L3 and the charged residues creating the central constriction region with the key regions, EV (extracellular vestibule), PR (preorientation region), CR (constriction region), PV (periplasmic region), view from the side and from the top. Bottom: structure of the selected penicillin molecules with their charge state at neutral pH; charged groups are highlighted in blue (positive) and red (negative).

Theoretical background

Bacterial porins function as non-specific channels and the passive mechanism of molecular permeability can be treated as a one-dimensional diffusion-drift problem.[45] Solving the Fick equation corrected with the drift motion due to pore-molecule interactions,[46] with the suitable boundary conditions for the diffusion of a molecule through a finite channel, the flux of molecules at equilibrium only depends on the diffusion constant of the molecule and its free energy along the diffusion axis:

View Article Online
DOI: 10.1039/D3CP02895J

$$J = -N_a S^0_{porin} \Delta c \left[\int_0^L \frac{\exp\left(\frac{U(z)}{k_B T}\right)}{D(z)} dz \right]^{-1} \quad (1)$$

where N_a is the Avogadro constant, S^0_{pore} is the geometrical cross section at the mouth of the channel and Δc is the difference of the solute molar concentrations. U(Z) is the potential of mean force, and D(Z) is the diffusion coefficient along the pore axis (Z); L is the length of the pore, and $k_B T$ is the thermodynamic temperature. U(Z) and D(Z) can be determined from all-atom MD simulations. There are two key points in Eq.1: (i) the flux depends on the integral along the entire axis of diffusion [0, L], meaning that we need to know the global free energy: thus, information about local high-affinity co-complex structures, such as those obtained with molecular docking, might be not sufficient to predict flux; (ii) the flux is a macroscopic property; hence it depends on the average over a high number of translocation events, expressed by the PMF U(Z), and a large sampling (dynamics) is required to predict permeability correctly. The global property and the statistical requirement for predicting the flux[47] together with the lack of a robust and direct method to measure permeability,[48] represents an obstacle in the drug discovery process to search for new antibiotics able to permeate through general porins, overcoming the OM of Gram-negative bacteria and reaching their targets within the bacterial cell.[49,50]

Free energy surfaces

We calculated the potential of mean force (PMF) for the translocation of each molecule through OmpF (**Fig.1**), using enhanced sampling techniques (metadynamics)[51] with two general collective variables (CV): the molecule position with respect to the main

axis Z of diffusion, reported in the Y-axis (**Fig. 1**) and the orientation of the beta-lactam ring, reported in the X-axis (**Fig.1**). Previous simulations of ampicillin through OmpF revealed an affinity site inside the CR due to the restriction of the sampled CV-space along Z.[52,53] The position of this binding site was not in agreement with the co-complex structure solved a posteriori for ampicillin inside OmpF, generating a controversial discussion around its location and the role it might have on transport.[21,22] Thanks to the computational advances, in this work we could afford to explore the entire CV-space that extends to the entire lumen, from the bulk in the EV (+40 Å) to the bulk in the PV (-30 Å), according to eqn. 1. As expected, the highest energy barrier is located in the CR because of the pore size exclusion filter, but with subtle differences from one molecule to another. In the case of ampicillin and benzylpenicillin the barrier extends from -10 Å $\leq z \leq$ 0 Å, while in the case of carbenicillin it extends on a larger region (-10 Å $\leq z \leq$ 10 Å). The cationic compound-1 exhibits the narrowest barrier (-3 Å $\leq z \leq$ 0 Å) when it penetrates with the positive groups ahead, while the barrier is slightly broad (-9 Å $\leq z \leq$ -3 Å) in the opposite case. These differences are correlated with the cation selectivity of the pore and in agreement with previous X-ray study on ion density.[54] The translocation of ampicillin and carbenicillin has been studied computationally in the past[52,53] and both molecules have been co-crystallized inside OmpF.[22] The minima corresponding to these two co-crystal structures are highlighted in orange in the free energy maps depicted in **Figure 2**, for ampicillin in the PR (**Fig.2a, 3a**) and in the PV for carbenicillin (**Fig.2d, 3d**), both corresponding to the global minimum of the conformational landscape. Although, there is not a co-crystal structure solved for benzylpenicillin inside OmpF (**Fig.2c, 3c**), we found a minimum for this molecule in the same region (EV) where a fragment of ertapenem (negatively charged as benzylpenicillin) has been co-crystallised inside OmpF,[22] though providing a low

View Article Online
DOI: 10.1039/D3CP02895J

resolution co-complex. The root mean square deviations (RMSD) from the co-crystal structures are remarkably good, 2.8 Å (**Fig. 3a, bottom**) in the case of ampicillin and 3.4 Å (**Fig. 3d, bottom**) in the case of carbenicillin. The latter value is apparently high since we predicted the binding with opposite orientation with respect to X-ray, though maintaining the main interactions of the (symmetrically placed) carboxylic charged groups of carbenicillin. In the case of benzylpenicillin we cannot estimate the RMSD with respect to the (low resolution) fragment of ertapenem, however the interacting residues are conserved (**Fig. 3c, bottom**). Despite there is not co-crystal structure available for the cationic compound-1, we found a minimum in the PR/CR interface, not far from the ampicillin binding site and in agreement with a pore that is cation selective.

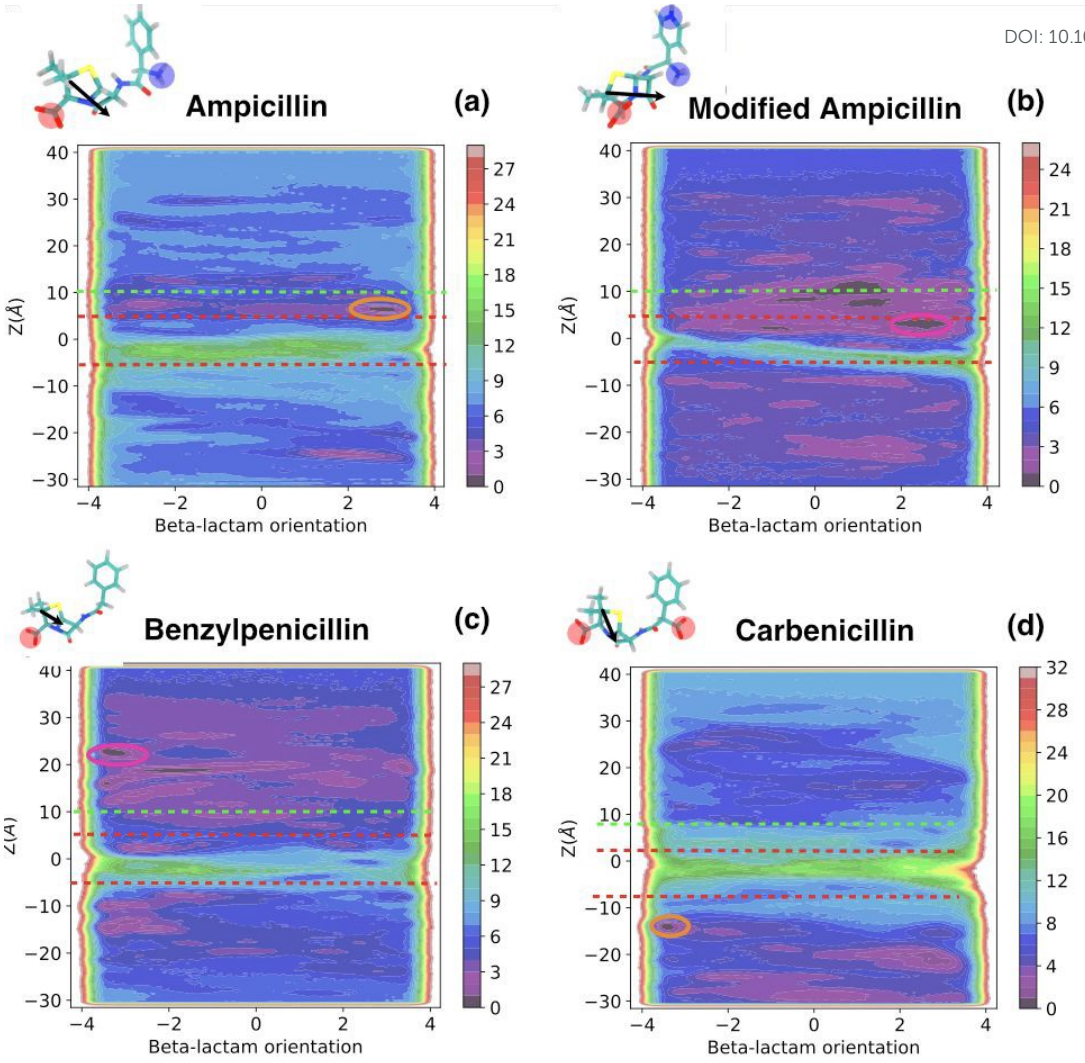

Figure 2. Free energy surface of the translocation of different beta-lactam antibiotics, namely: **(a)** Ampicillin, **(b)** cationic compound-1, **(c)** benzylpenicillin and **(d)** carbenicillin. Y-axis corresponds to Z coordinate (along the axis of diffusion) of the antibiotic and X-axis to the orientation of the beta-lactam ring. A positive value corresponds to the phenyl ring of the antibiotic pointing up towards the extracellular vestibule (EV) and a negative value indicates it is pointing down towards the periplasmic vestibule (PV). Zero values correspond to a situation in which the main axis of the beta-lactam ring is perpendicular to the axis of diffusion. Each line corresponds to a difference of 1 Kcal/mol. CR is located between -5.0 Å and 5.0 Å along the axis of diffusion (z). The pre-orientation region (PR) is highlighted just above the CR. Minima corresponding to co-crystal structures are highlighted in orange while other analysed minima are highlighted in magenta.

View Article Online
DOI: 10.1039/D3CP02895J

The main difference between the pose of the zwitterionic ampicillin and the cationic compound-1 form is caused by an additional interaction with a negatively charged residue from the loop L3 (E117, **Fig. 3b, bottom)**. Hence the conformation is shifted towards a more central position in the pore (**Fig. 3b, bottom**). Interestingly, the region where the zwitterionic and the cationic compound-1 bind in OmpF has been identified as a high-affinity site for the zwitterionic form of norfloxacin in OmpF.[10] The identified affinity sites are distributed along the axis of diffusion of the protein according to the charge state of the molecule, highlighting a non-specificity of interactions as well the importance of the internal electrostatics of the pore in its filtering mechanism.

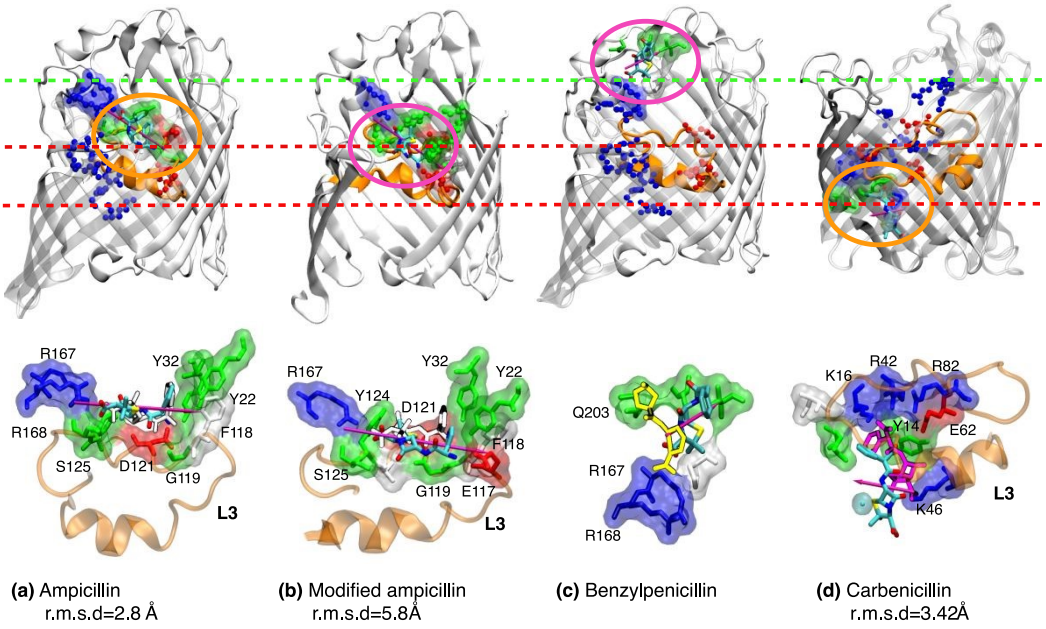

Figure 3. **Upper panel**: most relevant conformations from the selected free energy minima in Figure 1. The antibiotic conformation is depicted in licorice, with its electric dipole moment in magenta for (**a**) ampicillin, (**b**) cationic compound-1, (**c**) benzylpenicillin and (**d**) carbenicillin. The OmpF pore is represented as a white cartoon with the constricting loop (L3) highlighted in orange. The most relevant charged residues are highlighted in CPK representation and coloured according to their charge. The residues within a sphere of radius 4 Å centred in the antibiotic

are depicted as licorice, with its van der waals surface in a transparent material, and coloured according to its type. In the case of carbenicillin, the view is rotated by 90 degrees around the axis of diffusion. The different regions of the pore are labelled; the 'pre-orientation' region (PR) and the constriction region (CR) are highlighted following the colour scheme Figure 1. **Bottom panel**: the co-crystal structures for ampicillin depicted as white licorice **(a,b)**, ertapenem, yellow licorice **(c)** and carbenicillin, magenta licorice **(d)** are superimposed onto the conformations extracted from the metadynamics run. For ampicillin, cationic compound-1 and carbenicillin, the root mean square deviation (RMSD) from the crystal structure is indicated.

We calculated U(Z) from the projection of the computed PMF for the translocation of each molecule through OmpF onto the diffusion axis ($U_{metad}(Z)$, **Fig. 4**). As previously observed in the two-dimensional free energy map, the main barrier for translocation is located in the CR for all compounds.

This barrier has an entropic contribution, due to the limited configurational space available to the diffusing molecule when it enters the pore:

$$U(CR) - U(mouth) = -kTln\left(\frac{A(CR)}{A(mouth)}\right) \qquad (2)$$

where A is the effective area, in the plane transversal to the pore axis, available to the diffusing molecule. Eq. 2 is straightforward when the molecule has a size smaller than the pore. Here we are in the opposite condition: the average size of molecules is always larger than the average size of the pore in the constriction region. However, the molecule can permeate, when the pore expands and the molecule itself shrinks due to thermal fluctuations. Also, one can assume that the molecule enters the constriction region by aligning its long gyration axis with the pore axis. We suggested a statistical model taking these arguments into account[42] and the entropic barrier can be modelled as it follows, considering explicitly the fluctuations of the molecule and of the pore:

View Article Online
DOI: 10.1039/D3CP02895J

$$U_{steric}(z) = k_B T \frac{(R_{porin}(z) - R_{molecule})^2}{2(\sigma^2_{porin}(z) + \sigma^2_{molecule})} \quad (3)$$

where $R_{porin}(z) = \sqrt{\frac{S_{porin}(z)}{\pi}}$, being $S_{porin}(z)$ the minimal geometrical cross section of the pore along the diffusion axis, and $R_{molecule} = \sqrt{\frac{S_{molecule}}{\pi}}$, being $S_{molecule}$ the minimal projection area of the molecule.

The four ~~three~~ molecules selected have a similar size ($S_{ampicillin}$ = 50.5 Å^2, $S_{cationic\text{-}comp}$=49.5 Å^2, $S_{benzylpenicillin}$= 46.7 Å^2 and $S_{carbenicillin}$= 50.0 Å^2), hence the steric contribution calculated using Eq. 3 to the total free energy for translocation is very similar: ampicillin, cationic compound-1 and carbenicillin ~12 kcal/mol (**Fig. 4a,c**, red line); benzylpenicillin ~11 kcal/mol (**Fig. 4b**, red line). However, the one-dimensional free energy barriers calculated with metadynamics ($U_{metad}(Z)$, **Fig.4**, solid black line) are different for each molecule: ~4.5 kcal/mol for ampicillin, ~6.2 kcal/mol for benzylpenicillin and ~7.2 kcal/mol for carbenicillin. In the case of the cationic compound-1 the process can be considered almost barrier-less, ~1 kcal/mol, if we consider the statistical error is of the same magnitude.

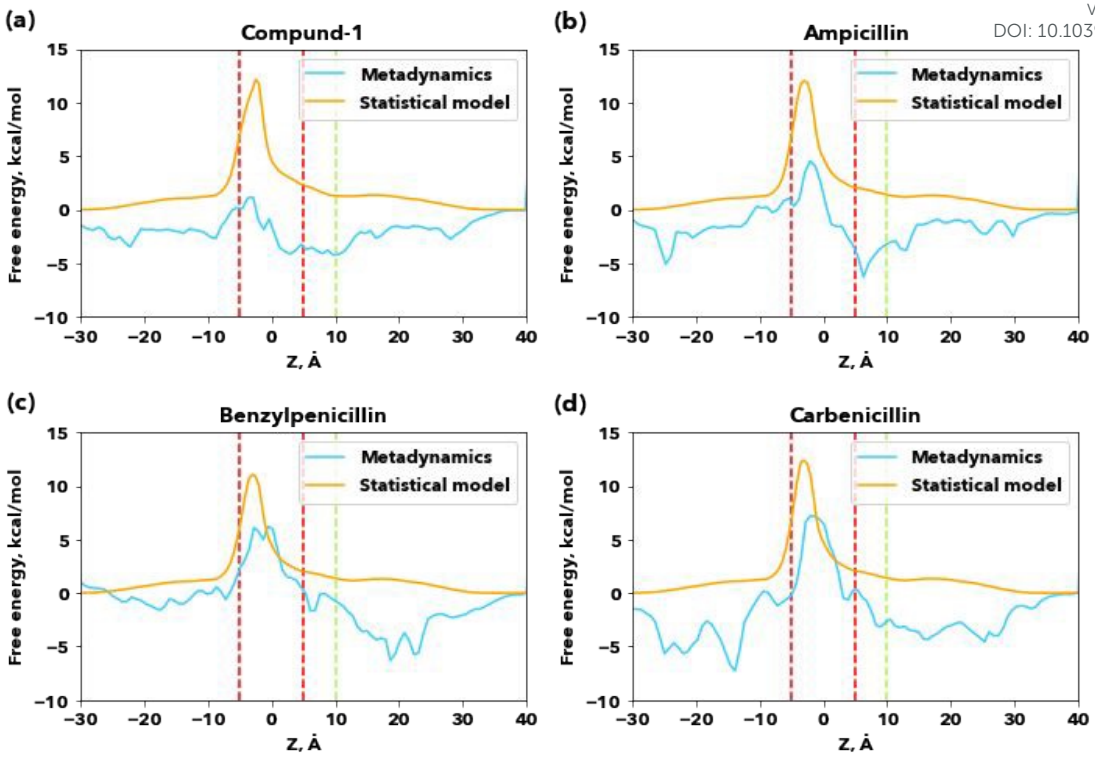

Figure 4. Projection of the free-energy surface, obtained with metadynamics (blue), along the diffusion axis and compared with the steric-entropic contribution (orange) to the free-energy for the four studied compounds: cationic compound-1 **(a)**, ampicillin **(b)**, benzylpenicillin **(c)** and carbenicillin **(d)**. The 'pre-orientation' region (PR) is highlighted in green, and the constriction region (CR) in red. The statistical model refers to the use of Eq. 3.

Table 1. Molecular parameters for the studied compounds and energy compensation calculated as the difference between the maximum of the steric-entropic contribution and the maximum of the total free energy obtained from metadynamics, derived from Figure 4.

	Size	Electric Dipole	Steric barrier	Total barrier	Energy compensation

	(A^2)	(Debye)	(kcal/mol)	(kcal/mol)	(kcal/mol)
Cationic compound-1 (+1)	49.5	37	12.2	1.1	11.1
Ampicillin (0, zwitterionic)	50.5	34	12.0	4.5	7.5
Benzylpenicillin (-1)	46.7	18.2	11.0	6.2	4.8
Carbenicillin (-2)	50	12.7	12.4	7.2	5.2

In this model the selectivity of the porin for cations[40] naturally arises from their interaction with the negative electric potential inside the CR. In the case of ampicillin (**Fig. 4a**) the electrostatic interaction of its electric dipole moment with the internal electric field reduces the steric barrier, a reduction of 7.5 kcal/mol, from 12 kcal/mol to 4.5 kcal/mol, and the deepest minimum along the one-dimensional free energy coincides for metadynamics at the co-crystal conformation, where the alignment of the dipole moment of ampicillin to the internal electric field of OmpF is optimal (**Fig. 3a**). For the anionic benzylpenicillin the contribution of the dipolar term to the reduction of the barrier is reduced by the repulsive charge/electrostatic potential additional interaction, a reduction of 4.8 kcal/mol, from 11 kcal/mol to 6.2 kcal/mol. The compensation is similar with the di-anionic carbenicillin, a reduction of 5.2 kcal/mol, from 12.4 kcal/mol to 7.2 kcal/mol, however with a total barrier higher because of the large steric term. Conversely, in the case of the cationic compound-1 the additional positive group compensates more the steric barrier, thus making the process almost barrierless, a reduction of 11.1 kcal/mol, from 12.2 kcal/mol to 1.1 kcal/mol. This

explain why modifying existing scaffolds by adding a positive group enhances intracellular accumulation of compounds in Gram-negative bacteria.[39,55]

Conclusion

We investigated the permeability of four related penicillin compounds through the model porin OmpF. These molecules were selected to have the same size and incremental electric charge and dipole moment, from -2e to +1e and from 12.7 D to 37 D. Our results show clearly how the free energy barrier for permeation is correlated with the increase of the charge (from negative to positive) and dipole moment. The sieving mechanism of porins goes beyond the size exclusion problem imposed by the CR. The entropic barrier keeps the permeation rate low, acting as a steric general filter. At the same time, the electrostatic interactions fine-tune selectivity and molecular transport in a specific way, as shown by the mutation of key charged residues in resistant mutants.[31] Thus, a rational distribution of charged groups in the molecule's scaffold, creating an electric dipole moment, might tremendously impact molecular permeability by tuning the central free energy barrier. Moreover, unlike specific channels, which require binding for successful translocation or permeation,[13,56] in general porins a free energy barrier controls permeability, with affinity sites becoming relevant for transport only at high concentrations when saturation occurs.[46,57]

Further, reminding that these porins are cation-selective (OmpF is slightly cation selective, 1.33 [40]), we showed that the presence of one or more positive groups in the scaffold could decrease the barrier because of the favoured interactions at the bottleneck or near the constriction region where the steric barrier occurs. In the past, the addition of a positive amine group in the scaffold resulted promising in converting an antibiotic effective against Gram-positive to a broad-spectrum antibiotic.[39] However, this is not

View Article Online
DOI: 10.1039/D3CP02895J

the only strategy to enhance the permeability of the scaffold in Gram-negative species since a large electric dipole, obtained by placing ad hoc charged groups can favor transport too.[58]

Note that to obtain a large electric dipole moment, we need to put far apart the positive and negative groups. Thus, it requires to have a large scaffold, which increases the steric barrier. It is not surprising that using our scoring function for predicting molecular permeability, we found that medium-size molecules have a better permeability, on average, than small-size molecules.[59] Eventually, it is the subtle balance between size and electrostatic that tunes the free energy barrier for permeation through porins into the periplasmic space.[40]

The main features of the OmpF filter (constriction size, rigidity and internal electrostatics) are appealing for technological applications: (i) having a barrier instead of a minimum to regulate permeation avoids saturation at high concentration; (ii) the permeation process does not involve large conformational changes, thus allowing fast rates of permeation; (iii) the electrostatic compensation is general and does not depend on specific chemical groups, only on general physical properties as dipole and charge; (iv) the two filters (steric and electrostatic) stay in the same region, reducing the dimension of the pore. The overall presented mechanism shades light into a paradigmatic porin-mediated molecular uptake and the possibility of turning nature into high-tech machinery.

Computational methods

The experimental X-ray structure of OmpF (PDB Id: 2OMF) was used as starting coordinates for molecular dynamics (MD) simulations. All the amino acid residues were simulated in the ionization state at neutral pH except for the E296, which was

protonated (net charge 0) as suggested by Varma et al.[60] The entire trimer was embedded in a pre-equilibrated POPC (1-palmitoyl-2-oleoyl-sn-glycero-3-phosphocholine) bilayer of 259 lipids and the system was oriented in order to center the protein at the origin of the coordinate system and align the channel along the z-axis (positive z: extracellular side; negative z: periplasmic side). 33 sodium ions were added to neutralize the system total charge. The system was solvated with ~17000 water molecules (initial simulation box size: 11x11x9 nm; total number of atoms: ~100k).

After 1 ps of energy minimization (conjugate gradients), a slow heating from 10 to 300 K was carried out for 1 ns. During this stage, positional restraints were applied on the protein α-carbons (all three dimensions) as well as on the lipids phosphorus atoms (along z only). After releasing the constraints on the POPC, an equilibration stage follows for 4 ns in the NPT ensemble at 1.0 bar and 300 K. Finally, 0.6 micro seconds MD simulations were performed in the NVT ensemble after the elimination of the protein restraints.

The NPT equilibration was performed with the program NAMD,[61] with 1.0 fs time-step, and treating long-range electrostatics with the soft particle mesh Ewald (SPME) method (64 grid points and order 4 with direct cutoff at 1.0 nm and 1.0 Å grid-size). Pressure control was applied using the Nose-Hoover extended Lagrangean method with isotropic cell, integrated with the Langevin Dynamics (200 fs and 100 fs of piston period and decay, respectively). The latter was also applied for temperature control with 200 fs thermostat damping time. Production run in the NVT ensemble was performed through the ACEMD code compiled for GPUs, by rescaling hydrogen mass to 4 au and increasing the time-step up to 4.0 fs.[62,63] The Langevin thermostat was used with 1 ps damping time. SPME was used to treat the electrostatics as for the equilibration stage.

View Article Online
DOI: 10.1039/D3CP02895J

The Amber99SB-ILDN force field[64] was used for the protein and lipids, and the TIP3P for waters.[65]

The GAFF force-field parameters[66] were used to describe ampicillin, benzylpenicillin, carbenicillin and piperacillin (PubChem: CID 6249, 5904, 20824,43672). Partial atomic charges were evaluated according to the RESP approach:[67] the molecule was first optimized at the HF/6-31G(d) level, up to a convergence in energy of 10^{-5} au, using the Gaussian03 package. Atomic RESP charges were derived from the electrostatic potential using the antechamber module of the AMBER package.[68]

Starting from the final configuration of the OmpF simulation described above, for the four antibiotics, the molecule was placed outside the lumen of the first monomer. The difference between the z-coordinate of the center of mass (com) of the antibiotic two-ring system and the z-coordinate of the com of the protein monomer was 25 Å. A thousand steps of energy minimization were performed. The equilibration stage followed for 1 ns in the NVT ensemble at 300 K as described hereinbefore. Well-tempered metadynamics[51,69] simulations were performed until the first effective translocation through the protein constriction region (CR) was observed. Then, four configurations were randomly selected for each compound, two with the antibiotic located in the extracellular vestibule (EV), two in the periplasmic vestibule (PV). Correspondingly, four multiple-walkers[70] were set to extend the metadynamics reconstruction of the free-energy surface (FES). Two biased collective variables were used, namely, the antibiotic position and orientation inside the channel. In practice, the 'position' Δz was defined as the difference of the z-coordinate between the com of the antibiotic and that of the first porin monomer. The 'orientation' was defined on the basis of the orientation of the rigid two-ring system, as the difference of the z-

coordinate between the lactam carbonyl carbon and the sulfur bonded carbon. We used either 4 or 8 walkers arriving to a total simulation time of 2.2 μs (ampicillin and compound-1), 2.8 μs (benzylpenicillin) and 3 μs (carbenicillin). During the metadynamics, energy biases were added every 2 ps to each collective variable (initial height 1.0 kcal/mol; σ = 0.25-0.08 Å for position and orientation, respectively). Well-tempered ΔT was 3000K. We calculated the statistical error on the reconstructed metadynamics free energy surfaces in one dimension. We used the estimator of Ref. [71], formula 22: we compared the reconstructed free energy with that estimated from the collective variable sampling, having a larger frequency than the bias. The average error is around 0.1 kcal/mol. This error does not take into account the force field approximations and the choice of collective variables, though when we bias explicitly two variables the convergence is better. In a similar paper, the authors investigates the permeation of phosphomycin with metadynamics biasing only the position along Z, obtaining an error lower than 0.8 kcal/mol.[43] Our estimate of the error considering all approximations is around 1 kcal/mol.

Acknowledgements

This research was partially supported by EU funding within the NextGeneration EU-MUR PNRR Extended Partnership initiative on Emerging Infectious Diseases (Project no. PE00000007, INF-ACT). IB was supported in part by the Agence Nationale de la Recherche (France), project ANR BRIDGE AAP CE29. S.A.G. acknowledges support from an AGAUR Beatriu de Pinós MSCA-COFUND Fellowship (project 2020-BP-00177).

Bibliography

1 Koebnik R, Locher KP, Gelder PV. Structure and function of bacterial outer membrane proteins: barrels in a nutshell. *Mol Microbiol* 2000; **37**: 239–253.

2 Luscher A, Moynié L, Auguste PS, Bumann D, Mazza L, Pletzer D *et al.* TonB-dependent receptor repertoire of pseudomonas aeruginosa for uptake of siderophore-drug conjugates. *Antimicrob Agents Chemother* 2018; **62**: e00097-18.

3 Vergalli J, Bodrenko IV, Masi M, Moynié L, Acosta-Gutierrez S, Naismith JH *et al.* Porins and small-molecule translocation across the outer membrane of Gram-negative bacteria. *Nat Rev Micro* 2020; **18**: 164–176.

4 Ouldali H, Sarthak K, Ensslen T, Piguet F, Manivet P, Pelta J *et al.* Electrical recognition of the twenty proteinogenic amino acids using an aerolysin nanopore. *Nat Biotechnol* 2020; **38**: 176–181.

5 Zernia S, Heide NJVD, Galenkamp NS, Gouridis G, Maglia G. Current Blockades of Proteins inside Nanopores for Real-Time Metabolome Analysis. *ACS Nano* 2020; **14**: 2296–2307.

6 Bayley H. Nanopore sequencing: From imagination to reality. *Clin Chem* 2015; **61**: 25–31.

7 Shen J, Roy A, Joshi H, Samineni L, Ye R, Tu Y-M *et al.* Fluorofoldamer-Based Salt- and Proton-Rejecting Artificial Water Channels for Ultrafast Water Transport. *Nano Lett* 2022; **22**: 4831–4838.

8 Siria A, Bocquet M-L, Bocquet L. New avenues for the large-scale harvesting of blue energy. *Nature Reviews Chemistry* 2017; **1**: 0091.

9 Nikaido H. Molecular basis of bacterial outer membrane permeability revisited. *Microbiol Mol Biol Rev* 2003; **67**: 593–656.

10 Bajaj H, Acosta-Gutierrez S, Bodrenko I, Malloci G, Scorciapino MA, Winterhalter M *et al.* Bacterial Outer Membrane Porins as Electrostatic Nanosieves: Exploring Transport Rules of Small Polar Molecules. *ACS Nano* 2017; **11**: 5465–5473.

11 Groot BL de, Grubmüller H. Water permeation across biological membranes: mechanism and dynamics of aquaporin-1 and GlpF. *Science* 2001; **294**: 2353–2357.

12 Benz R, Schmid A, Vos-Scheperkeuter GH. Mechanism of sugar transport through the sugar-specific LamB channel of Escherichia coli outer membrane. *J Membr Biol* 1987; **100**: 21–29.

13 Dutzler R, Schirmer T, Karplus M, Fischer S. Translocation mechanism of long sugar chains across the maltoporin membrane channel. *Structure* 2002; **10**: 1273–1284.

14 Liu J, Eren E, Vijayaraghavan J, Cheneke BR, Indic M, Berg B van den *et al.* OccK channels from Pseudomonas aeruginosa exhibit diverse single-channel electrical signatures but conserved anion selectivity. *Biochemistry* 2012; **51**: 2319–2330.

15 Samanta S, Scorciapino MA, Ceccarelli M. Molecular basis of substrate translocation through the outer membrane channel OprD of Pseudomonas aeruginosa. *Phys Chem Chem Phys* 2015; **17**: 23867–23876.

16 Zahn M, Bhamidimarri SP, Baslé A, Winterhalter M, Berg B van den. Structural Insights into Outer Membrane Permeability of Acinetobacter baumannii. *Structure* 2016; **24**: 221–231.

17 Benkerrou D, Ceccarelli M. Free energy calculations and molecular properties of substrate translocation through OccAB porins. *Phys Chem Chem Phys* 2018; **20**: 8533–8546.

18 Samanta S, Bodrenko I, Acosta-Gutierrez S, D'Agostino T, Pathania M, Ghai I *et al.* Getting Drugs through Small Pores: Exploiting the Porins Pathway in Pseudomonas aeruginosa. *ACS Infect Dis* 2018; **4**: 1519–1528.

19 Pathania M, Acosta-Gutierrez S, Bhamidimarri SP, Baslé A, Winterhalter M, Ceccarelli M *et al.* Unusual Constriction Zones in the Major Porins OmpU and OmpT from Vibrio cholerae. *Structure* 2018; **26**: 1–14.

20 Ferrara LGM, Wallat GD, Moynié L, Dhanasekar NN, Aliouane S, Acosta-Gutierrez S *et al.* MOMP from Campylobacter jejuni Is a Trimer of 18-Stranded β-Barrel Monomers with a Ca(2+) Ion Bound at the Constriction Zone. *J Mol Biol* 2016; **428**: 4528–4543.

21 Kojima S, Nikaido H. Permeation rates of penicillins indicate that Escherichia coli porins function principally as nonspecific channels. *Proceedings of the National Academy of Sciences* 2013; **110**: E2629-34.

22 Ziervogel BK, Roux B. The Binding of Antibiotics in OmpF Porin. *Structure/Folding and Design* 2012; **21**: 1–12.

23 Acosta-Gutierrez S, Bodrenko I, Scorciapino MA, Ceccarelli M. Macroscopic electric field inside water-filled biological nanopores. *Phys Chem Chem Phys* 2016; **18**: 8855–8864.

24 Nakae T, Nikaido H. Outer membrane as a diffusion barrier in Salmonella typhimurium. Penetration of oligo- and polysaccharides into isolated outer membrane vesicles and cells with degraded peptidoglycan layer. *J Biol Chem* 1975; **250**: 7359–7365.

25 Pagès J-M, James CE, Winterhalter M. The porin and the permeating antibiotic: a selective diffusion barrier in Gram-negative bacteria. *Nat Rev Micro* 2008; **6**: 893–903.

26 Ujwal R, Cascio D, Colletier J-P, Faham S, Zhang J, Toro L *et al.* The crystal structure of mouse VDAC1 at 2.3 Å resolution reveals mechanistic insights into metabolite gating. *Proc National Acad Sci* 2008; **105**: 17742–17747.

27 Amodeo GF, Scorciapino MA, Messina A, Pinto VD, Ceccarelli M. Charged residues distribution modulates selectivity of the open state of human isoforms of the voltage dependent anion-selective channel. *PLoS ONE* 2014; **9**: e103879.

28 Vikraman D, Satheesan R, Rajendran M, Kumar NA, Johnson JB, R SK *et al.* Selective Translocation of Cyclic Sugars through Dynamic Bacterial Transporter. *Acs Sensors* 2022; **7**: 1766–1776.

29 Vasan AK, Haloi N, Ulrich RJ, Metcalf ME, Wen P-C, Metcalf WW *et al.* Role of internal loop dynamics in antibiotic permeability of outer membrane porins. *Proceedings of the National Academy of Sciences* 2022; **119**: e2117009119.

30 Milenkovic S, Wang J, Acosta-Gutierrez S, Winterhalter M, Ceccarelli M, Bodrenko IV. How the physical properties of bacterial porins match environmental conditions. *Phys Chem Chem Phys* 2023; **25**: 12712–12722.

31 Lou H, Chen M, Black SS, Bushell SR, Ceccarelli M, Mach T *et al.* Altered Antibiotic Transport in OmpC Mutants Isolated from a Series of Clinical Strains of Multi-Drug Resistant E. coli. *PLoS ONE* 2011; **6**: e25825.

32 Acosta-Gutierrez S, Scorciapino MA, Bodrenko I, Ceccarelli M. Filtering with Electric Field: The Case of E. coli Porins. *J Phys Chem Lett* 2015; **6**: 1807–1812.

33 Singh PR, Ceccarelli M, Lovelle M, Winterhalter M, Mahendran KR. Antibiotic permeation across the OmpF channel: modulation of the affinity site in the presence of magnesium. *J Phys Chem B* 2012; **116**: 4433–4438.

34 López ML, García-Giménez E, Aguilella VM, Alcaraz A. Critical assessment of OmpF channel selectivity: merging information from different experimental protocols. *J Phys Condens Matter* 2010; **22**: 454106.

35 Chowdhury R, Ren T, Shankla M, Decker K, Grisewood M, Prabhakar J *et al.* PoreDesigner for tuning solute selectivity in a robust and highly permeable outer membrane pore. *Nature Communications* 2018; **9**: 3661–10.

36 Parker EN, Drown BS, Geddes EJ, Lee HY, Ismail N, Lau GW *et al.* Implementation of permeation rules leads to a FabI inhibitor with activity against Gram-negative pathogens. *Nat Microbiol* 2020; **5**: 67–75.

37 Westfall DA, Krishnamoorthy G, Wolloscheck D, Sarkar R, Zgurskaya HI, Rybenkov VV. Bifurcation kinetics of drug uptake by Gram-negative bacteria. *PLoS ONE* 2017; **12**: e0184671.

38 Kullman L, Winterhalter M, Bezrukov SM. Transport of maltodextrins through maltoporin: a single-channel study. *Biophys J* 2002; **82**: 803–812.

39 Richter MF, Drown BS, Riley AP, Garcia A, Shirai T, Svec RL *et al.* Predictive compound accumulation rules yield a broad-spectrum antibiotic. *Nature Publishing Group* 2017; **545**: 299–304.

40 Acosta-Gutierrez S, Ferrara L, Pathania M, Masi M, Wang J, Bodrenko I *et al.* Getting Drugs into Gram-Negative Bacteria: Rational Rules for Permeation through General Porins. *ACS Infect Dis* 2018; **4**: 1487–1498.

41 Gutiérrez SA, Bodrenko I, Ceccarelli M. Permeability Through Bacterial Porins Dictates Whole Cell Compound Accumulation. 2020. doi:10.26434/chemrxiv.11877834.

42 Bodrenko IV, Salis S, Acosta-Gutierrez S, Ceccarelli M. Diffusion of large particles through small pores: From entropic to enthalpic transport. *J Chem Phys* 2019; **150**: 211102.

43 Golla VK, Prajapati JD, Joshi M, Kleinekathöfer U. Exploration of Free Energy Surfaces Across a Membrane Channel Using Metadynamics and Umbrella Sampling. *J Chem Theory Comput* 2020; **16**: 2751–2765.

44 Lapierre J, Hub JS. Converging PMF Calculations of Antibiotic Permeation across an Outer Membrane Porin with Subkilocalorie per Mole Accuracy. *J Chem Inf Model* 2023; **63**: 5319–5330.

45 Bezrukov SM, Berezhkovskii AM, Szabo A. Diffusion model of solute dynamics in a membrane channel: Mapping onto the two-site model and optimizing the flux. *J Chem Phys* 2007; **127**: 115101.

46 Bodrenko IV, Milenkovic S, Ceccarelli M. Diffusion of molecules through nanopores under confinement: Time-scale bridging and crowding effects via Markov state model. *Biomol Concepts* 2022; **13**: 207–219.

47 Scorciapino MA, Acosta-Gutierrez S, Benkerrou D, D'Agostino T, Malloci G, Samanta S *et al.* Rationalizing the permeation of polar antibiotics into Gram-negative bacteria. *J Phys Condens Matter* 2017; **29**: 113001.

48 Winterhalter M, Ceccarelli M. Physical methods to quantify small antibiotic molecules uptake into Gram-negative bacteria. *Eur J Pharm Biopharm* 2015; **95**: 63–67.

49 Payne DJ, Gwynn MN, Holmes DJ, Pompliano DL. Drugs for bad bugs: confronting the challenges of antibacterial discovery. *Nat Rev Drug Discov* 2007; **6**: 29–40.

50 Tommasi R, Brown DG, Walkup GK, Manchester JI, Miller AA. ESKAPEing the labyrinth of antibacterial discovery. *Nat Rev Drug Discov* 2015; **14**: 529–542.

DOI: 10.1039/D3CP02895J

51 Laio A, Parrinello M. Escaping free-energy minima. *Proc Natl Acad Sci USA* 2002; **99**: 12562–12566.

52 Danelon C, Nestorovich EM, Winterhalter M, Ceccarelli M, Bezrukov SM. Interaction of zwitterionic penicillins with the OmpF channel facilitates their translocation. *Biophys J* 2006; **90**: 1617–1627.

53 Kumar A, Hajjar E, Ruggerone P, Ceccarelli M. Molecular simulations reveal the mechanism and the determinants for ampicillin translocation through OmpF. *J Phys Chem B* 2010; **114**: 9608–9616.

54 Im W, Roux B. Ion permeation and selectivity of OmpF porin: a theoretical study based on molecular dynamics, Brownian dynamics, and continuum electrodiffusion theory. *J Mol Biol* 2002; **322**: 851–869.

55 Perlmutter SJ, Geddes EJ, Drown BS, Motika SE, Lee MR, Hergenrother PJ. Compound Uptake into E. coli Can Be Facilitated by N-Alkyl Guanidiniums and Pyridiniums. *ACS Infect Dis* 2021; **7**: 162–173.

56 Coines J, Acosta-Gutierrez S, Bodrenko I, Rovira C, Ceccarelli M. Glucose transport via the pseudomonad porin OprB: implications for the design of Trojan Horse anti-infectives. *Phys Chem Chem Phys* 2019; **21**: 8457–8463.

57 Berezhkovskii AM, Bezrukov SM. Optimizing transport of metabolites through large channels: molecular sieves with and without binding. *Biophys J* 2005; **88**: L17-9.

58 Durand-Reville TF, Miller AA, O'Donnell JP, Wu X, Sylvester MA, Guler S *et al.* Rational design of a new antibiotic class for drug-resistant infections. *Nature Publishing Group* 2021; **597**: 698–702.

59 Acosta-Gutierrez S, Bodrenko IV, Ceccarelli M. The Influence of Permeability through Bacterial Porins in Whole-Cell Compound Accumulation. *Antibiotics (Basel)* 2021; **10**: 635.

60 Varma S, Chiu S-W, Jakobsson E. The influence of amino acid protonation states on molecular dynamics simulations of the bacterial porin OmpF. *Biophys J* 2006; **90**: 112–123.

61 Phillips JC, Braun R, Wang W, Gumbart J, Tajkhorshid E, Villa E *et al.* Scalable molecular dynamics with NAMD. *J Comput Chem* 2005; **26**: 1781–1802.

62 Harvey MJ, Fabritiis GD. An implementation of the smooth particle mesh Ewald method on GPU hardware. *J Chem Theory Comput* 2009; **5**: 2371–2377.

63 Harvey MJ, Giupponi G, Fabritiis GD. ACEMD: accelerating biomolecular dynamics in the microsecond time scale. *J Chem Theory Comput* 2009; **5**: 1632–1639.

DOI: 10.1039/D3CP02895J

64 Lindorff-Larsen K, Piana S, Palmo K, Maragakis P, Klepeis JL, Dror RO *et al.* Improved side-chain torsion potentials for the Amber ff99SB protein force field. *Proteins* 2010; **78**: 1950–1958.

65 Jorgensen WL, Chandrasekhar J, Madura JD, Impey RW, Klein ML. Comparison of simple potential functions for simulating liquid water. *J Chem Phys* 1983; **79**: 926.

66 Wang J, Wolf RM, Caldwell JW, Kollman PA, Case DA. Development and testing of a general amber force field. *Journal of Computational Chemistry* 2004; **25**: 1157–1174.

67 Bayly CI, Cieplak P, Cornell W, Kollman PA. A well-behaved electrostatic potential based method using charge restraints for deriving atomic charges: the RESP model. *J Phys Chem* 1993; **97**: 10269–10280.

68 Case DA, Cheatham TE, Darden T, Gohlke H, Luo R, Merz KM *et al.* The Amber biomolecular simulation programs. *J Comput Chem* 2005; **26**: 1668–1688.

69 Barducci A, Bussi G, Parrinello M. Well-Tempered Metadynamics: A Smoothly Converging and Tunable Free-Energy Method. *Phys Rev Lett* 2008; **100**: 1–4.

70 Raiteri P, Laio A, Gervasio FL, Micheletti C, Parrinello M. Efficient reconstruction of complex free energy landscapes by multiple walkers metadynamics. *The journal of physical chemistry B, Condensed matter, materials, surfaces, interfaces & biophysical* 2006; **110**: 3533–3539.

71 Branduardi D, Bussi G, Parrinello M, 2012. Metadynamics with adaptive Gaussians. *Journal of Chemical Theory and Computation*; **8**: 2247–2254.